Solid-State ^{77}Se NMR and XRD Study of the Structure and Dynamics of Seleno-Oxyanions in Hydrotalcite-like Compounds

Xiaoqiang Hou* and R. James Kirkpatrick

Department of Geology, University of Illinois at Urbana-Champaign, Urbana, Illinois 61801

Received December 20, 1999. Revised Manuscript Received April 14, 2000

We report here the first ^{77}Se nuclear magnetic resonance (NMR) and XRD study of the dynamical and structural behavior of selenate and selenite in hydrotalcite-like compounds (HT-SeO_4 and HT-SeO_3). The swelling properties and dynamical behavior of the anions in HT-SeO_4 and HT-SeO_3 are very different, and the results provide significant new insight into the structure and dynamical behavior of the interlayer and surface anions of this important group of compounds. HT-SeO_4 expands from a one water layer to two water layer structure in response to increasing relative humidity, and the structural transition is captured by both the ^{77}Se chemical shift anisotropy (CSA) and the basal lattice spacing. Although selenate is a tetrahedral anion, the observed ^{77}Se CSA is uniaxial, probably due to the combined effects of hydrogen bonding to the hydroxyls of octahedral layer and the H atoms of interlayer waters, and Coulombic interaction with the positive charge of the main layer. The selenate reorientation frequency follows an Arrhenius relationship. The reorientation frequencies are higher and the apparent activation energy lower for unrecrystallized samples with relatively small particle size than for recrystallized samples with relatively large particle size. These observations and the lack of a well-defined CSA pattern for the unrecrystallized sample suggest that the spectra of the recrystallized samples are dominated by signals from interlayer selenate, whereas those of the unrecrystallized samples are dominated by signals from surface selenate and selenate in disordered interlayers. In contrast, HT-SeO_3 does not expand with increasing relative humidity, and spectroscopically resolvable surface-absorbed and interlayer selenite have dramatically different dynamical characteristics. The interlayer selenite shows a well-defined, relative humidity (RH)-independent uniaxial chemical shift anisotropy (CSA) powder pattern, indicating that it is rigidly held or perhaps rotating on its 3-fold axis at all hydration conditions at room temperature, consistent with the observed lack of expansion. For surface selenite, however, the reorientation frequency increases substantially with increasing relative humidity. Because selenium and sulfur have many similar properties and HT-SO_4 and HT-SeO_4 both expand with increasing RH, the ^{77}Se NMR data reported here are likely to be relevant to understanding the behavior of sulfate and sulfite HTs.

Introduction

Hydrotalcite-like compounds (HTs, also known as mixed-metal layered hydroxides, layered double hydroxides and anionic clays) are layer-structure hydroxides with permanent, positive layer charge and significant anion-exchange capacity.[1−7] Their crystal structures consist of single brucite-like octahedral layers alternating with interlayers containing exchangeable anions and water, and they develop layer charge by isomorphous cation substitution in the hydroxide layer. For many HTs, the general formula is $M_{1-x}^{2+}M_x^{3+}(OH)_2 \cdot A_{x/n}^{n-} \cdot mH_2O$, and numerous studies have shown extensive solid solution on all sites.[1,6,7] A^{n-} can be a wide range of inorganic anions, organic anions, and complexes.[2−8] Different stackings of the hydroxide layers results in different polytypes (e.g., 2H, 3R), illite/smectite (I/S)-like ordered interstratification is possible, and turbostratic disorder is common.[1] Because of the large surface areas of HTs (up to 80 m^2/g; e.g., ref 3), surface-adsorbed anions are often important and can have significantly different dynamic behavior than interlayer anions.[9,10]

HTs are widely used as catalysts and catalyst precursors[1] and also have potential applications in hazardous waste management,[11−21] electrochemistry[22,23] and medi-

* Corresponding author. Phone: (217) 244-2355. Fax: (217) 244-4996. E-mail: xhou@uiuc.edu.

(1) Cavani, F.; Trifiro, F.; Vaccari, A. *Catal. Today* **1991**, *11*, 173.
(2) Miyata, S. *Clays Clay Miner.* **1975**, *23*, 369.
(3) Miyata, S. *Clays Clay Miner.* **1980**, *28*, 50.
(4) Miyata, S. *Clays Clay Miner.* **1983**, *31*, 305.
(5) Miyata, S.; Okada, A. *Clays Clay Miner.* **1977**, *25*, 14.
(6) Newman, S. P.; Jones, W. *New J. Chem.* **1998**, 105.
(7) Mitchell, I. V. *Pillared Layered Structures: Current Trends and Applications*; Elsevier Science Publishers: New York, 1990.
(8) Gardner, E. A.; Yun, S. K.; Kwon, T.; Pinnavaia, T. J. *Appl. Clay Sci.* **1998**, *13* (5−6), 479.
(9) Kirkpatrick, R. J.; Yu, P.; Hou, X.; Kim, Y. *Am. Mineral.* **1999**, *84* (7−8), 1186.
(10) Hou, X.; Kirkpatrick, R. J.; Yu, P.; Moore, D.; Kim, Y. *Am. Mineral.* **2000**, *85*, 173.
(11) Amin, S.; Jayson, G. G. *Water Res.* **1996**, *30* (2), 299.

10.1021/cm990787w CCC: $19.00
Published on Web 06/02/2000

cine.[24] Their compositional variability offers substantial flexibility to tailor them to specific requirements. Recent research has also shown that HTs can form on the surfaces of oxide and clay minerals during reaction with heavy metal cations, suggesting a potential route for heavy metal sequestration in the environment.[25]

As for aluminosilicate clay minerals, many properties of HTs are related to the structural and dynamical behavior of interlayer and surface species, but due to small particle sizes and structural disorder, these species are difficult to study. XRD provides limited and uncertain molecular-scale information because of structural disorder. In contrast, nuclear magnetic resonance (NMR) spectroscopy has shown remarkable capacity to illuminate the local structure and dynamics of surface and interlayer anions on and in HTs.[9,10] Here we use ^{77}Se NMR and powder XRD to investigate the molecular-scale structure and dynamics of selenate (SeO_4^{2-}) and selenite (SeO_3^{2-}) in and on HTs. To our knowledge these are the first ^{77}Se NMR data for HTs or similar Se-containing phases. ^{77}Se has nuclear spin $I = {}^1/_2$ and a 7.86% natural abundance. Thus, it does not suffer quadrupolar peak distortion and is relatively easy to observe. Selenate and selenite are of significant environmental concern,[26] and understanding their molecular-scale behavior is essential to fundamental prediction and analysis of their exchange and adsorption behavior, which are closely related to their mobility, bioavailability, and recoverability. Because of their large exchange capacity, HTs provide ideal model systems for studying the structure and dynamics of the Se-oxyanions interacting with solids. In addition, understanding the behavior of these species is essential to comprehensive understanding of the behavior of interlayer species in HTs and intercalated species in layer-structure materials more generally.

Because sulfur does not have a readily accessible NMR-active nuclide but is chemically similar to selenium, selenate, and selenite may serve as effective model molecules for sulfate and sulfite, respectively. Selenite and sulfite, unlike nitrate, are not planar. Rather the Se and S atoms are displaced 0.80 and 0.72 Å, respectively, to one side of the plane of the three oxygen atoms.[27,28] The Se−O bond distance[27] in selenite is 1.70 Å compared to the S−O distance of 1.54 Å in sulfite.[28] Selenate and sulfate are both tetrahedral,[29] and the Se−O bond in selenate is typically about 1.65 Å compared to 1.43−1.49 Å for the S−O bond in sulfate.[30,31]

Experimental Methods

Sample Preparation. HT-SeO_4 and HT-SeO_3 were prepared by exchanging selenate and selenite for chloride in HT-Cl. Parent HT-Cl was synthesized from a $MgCl_2 \cdot 6H_2O$ and $AlCl_3 \cdot 6H_2O$ solution with a nominal Mg/Al molar ratio of 3 at 55 °C using the method of coprecipitation.[2,10] To decrease the ^{77}Se T_1 relaxation time for ^{77}Se NMR data collection, Fe^{3+} was added to the initial reaction mixture at a molar ratio of 0.1% of the total cations. After dropwise mixing, the precipitates were aged in the mixing solution at room temperature for 20 h in flowing nitrogen in a glovebag. The precipitates were then centrifugally separated and ultrasonically washed with three cycles to remove excess chloride. The freshly prepared HT-Cl was divided into several aliquots. Two of these were added separately to 0.2 M Na_2SeO_4 and 0.2 M Na_2SeO_3 solutions to allow exchange at 55 °C under vigorous stirring for 48 h. The exchanged samples were washed with three cycles as described above for HT-Cl. Half of each sample was then dried at 70 °C for 24 h in a vacuum oven. The samples obtained at this stage are referred to as unrecrystallized HT-SeO_4 and HT-SeO_3. They were analyzed for bulk chemical composition and investigated by powder X-ray diffraction (XRD), scanning electron microscopy (SEM) and ^{77}Se NMR. The other half of each sample was placed into boiled DI water and hydrothermally treated under autogenous pressure in a Parr vessel for 72 h at 200 °C to increase the particle size. The resulting products are referred to as recrystallized HT-SeO_4 and HT-SeO_3 and are the primary focus of the research. They were examined by elemental analysis, XRD, TGA, SEM, and ^{77}Se NMR. On the basis of our ^{77}Se NMR spectra and XRD data, about 10% of the SeO_3^{2-} in the HT-SeO_3 was oxidized to SeO_4^{2-} during the hydrothermal treatment. To reduce this oxidation, an aliquot of a newly made HT-Cl was first hydrothermally treated, and portions of the recrystallized HT-Cl were then separately exchanged with SeO_4^{2-} and SeO_3^{2-} in the way described above. The HT-SeO_4 sample prepared in this way is similar in all respects to the recrystallized HT-SeO_4 prepared by the first route, but the second HT-SeO_3 has less SeO_4^{2-} than the first. A flowing N_2 atmosphere and N_2-bubbled boiled water were used during the entire precipitation and washing process to minimize carbonate contamination, but the samples were exposed to air during sample loading and unloading and when exposed to RH buffers.

Sample Examination. Samples were examined using a Hitachi-S4700 scanning electron microscope at an accelerating voltage of 10 kV. For elemental analysis, the metallic elements and Se were determined using inductively coupled plasma emission spectroscopy (ICP), and C and H were determined with a CHN analyzer. TGA data were recorded from room temperature to 650 °C at a heating rate 5 °C/min under N_2 atmosphere. Powder XRD patterns of dried powders and water−HT pastes were recorded using a Scintag diffractometer using Cu Kα radiation. KGa-1 kaolinite (Clay Minerals Repository, University of Missouri—Columbia) was sometimes added as an internal standard. NMR spectra were collected at $H_0 = 11.7$ T under both static and MAS conditions using spectrometers equipped with Techmag Aries or Libra data systems, a Doty Scientific MAS probe, and a home-built static

(12) Balsley, S. D.; Brady, P. V.; Krumhansl, J. L.; Anderson, H. L. *J. Soil Contam.* **1998**, *7* (2), 125.
(13) Fetter, G.; Olguin, M. T.; Bosch, P.; Lara, V. H.; Bulbulian, S. *J. Radioanal. Nucl. Chem.* **1999**, *241* (3), 595.
(14) Hermosin, M. C.; Pavlovic, I.; Ulibarri, M. A.; Cornejo, J. *J. Environ. Sci. Health, Part A* **1993**, *28* (9), 1875.
(15) Houri, B.; Legrouri, A.; Barroug, A.; Forano, C.; Besse, J. P. *Collect. Czech. Chem. Commun.* **1998**, *63* (5), 732.
(16) Lakraimi, M.; Legrouri, A.; Barroug, A.; de Roy, A.; Besse, J. P. *J. Chim. Phys. Phys.-Chim. Biol.* **1999**, *96* (3), 470.
(17) Lehmann, M.; Zouboulis, A. I.; Matis, K. A. *Chemosphere* **1999**, *39* (6), 881.
(18) Narita, E.; Yamagishi, T.; Tazawa, K.; Ichijo, O.; Umetsu, Y. *Clay Sci.* **1995**, *9*, 187.
(19) Parker, L. M.; Milestone, N. B.; Newman, R. H. *Ind. Eng. Chem. Res.* **1995**, *34*, 1196.
(20) Ulibarri, M. A.; Pavlovic, I.; Hermosin, M. C.; Cornejo, J. *Appl. Clay Sci.* **1995**, *10*, 131.
(21) Villa, M. V.; Sanchez-Martin, M. J.; Sanchez-Camazano, M. *J. Environ. Sci. Health, Part B* **1999**, *34* (3), 509.
(22) Ballarin, B.; Gazzano, M.; Seeber, R.; Tonelli, D.; Vaccari, A. *J. Electroanal. Chem.* **1998**, *445* (1−2), 27.
(23) Qiu, J. B.; Villemure, G. *J. Electroanal. Chem.* **1997**, *428* (1−2), 165−172.
(24) Playle, A. C.; Gunning, S. R.; Llewellyn, A. F. *Pharm. Acta Helv.* **1974**, *49*, 298.
(25) Scheidegger, A. M.; Strawn, D. G.; Lamble, G. M.; Sparks, D. L. *Geochim. Cosmochim. Acta* **1998**, *62* (13), 2233.
(26) Yang, J.; Conver, T. S.; Koropchak, J. A. *Anal. Chem.* **1996**, *68* (22), 4064.
(27) Calculated on the basis of *Struct, Rep.* **1986**, *53A*, 239.
(28) Magnusson, A.; Johansson, L.-G.; Lindqvist, O. *Acta. Crystallogr.* **1981**, *B37*, 1108.
(29) Beagly, B.; Banks, E. *Struct. Rep.* **1963**, *28*, 222.

probe. Carrier frequencies of 95.435 or 95.417 MHz were applied for HT-SeO_3 and HT-SeO_4 respectively. The 90° pulse length was generally 7 μs. The recycle time was typically 1 s, but values up to 5 s were used to investigate T_1 relaxation effects on spectral intensity. No appreciable difference in line shapes or signal/noise ratios were found for spectra collected using these two recycle delays. The number of scans varied from ~1000 to 30 000. Solution Na_2SeO_4 (1 M) or Na_2SeO_3 (1 M) were used as external chemical shift standards, and their chemical shifts were set at 1051 and 1292 ppm respectively.[32] Variable-temperature spectra were collected from +100 to −100 °C using a liquid nitrogen cooling system and a resistance heating system. For spectra collected at room temperature and controlled RH, the samples were placed in open containers, equilibrated for at least 3 weeks over saturated salt buffers,[33] and quickly loaded into glass tubes (or MAS rotors) and sealed with epoxy just before data collection. ^{77}Se NMR spectra were also collected for HTs mixed with water to make thick pastes.

Results and Spectral Interpretation

Chemical Analysis and SEM Observation. The structural formulas based on elemental analysis are as follows: unrecrystallized HT-SeO_3, $Mg_{0.741}Al_{0.258}Fe_{0.001}(OH)_2(SeO_3)_{0.120}(CO_3)_{0.009}\cdot 0.650H_2O$; recrystallized HT-$SeO_3$, $Mg_{0.743}Al_{0.256}Fe_{0.001}(OH)_2(SeO_3)_{0.118}(CO_3)_{0.011}\cdot 0.646H_2O$; unrecrystallized HT-$SeO_4$, $Mg_{0.743}Al_{0.256}Fe_{0.001}(OH)_2(SeO_4)_{0.113}(CO_3)_{0.016}\cdot 0.739H_2O$; and recrystallized HT-$SeO_4$, $Mg_{0.763}Al_{0.236}Fe_{0.001}(OH)_2(SeO_4)_{0.104}(CO_3)_{0.015}\cdot 0.660H_2O$. These compositions conform to the desired stoichiometric compositions within analytical error except for the carbonate in all samples. Chlorine is below the detection limit, indicating that the exchange of the Se species for Cl^- is complete. The number of water molecules includes both absorbed water on external particle surfaces and interlayer water. The recrystallized samples have less water than the unrecrystallized samples, especially so for the HT-SeO_4 pair, as expected. Microscopically, the samples are poorly dispersed and occur mostly as aggregates of roughly circular or irregular platelets. The crystallites in the recrystallized samples are typically 500−1000 nm across and <30 nm thick. In the unrecrystallized samples, they are smaller and thinner. Well-crystallized hexagonal platelets are observed in the recrystallized samples but are not common.

XRD. *Ambient Conditions.* The random orientation powder XRD patterns of the samples (Figure 1) show only hydrotalcite phases, consistent with ^{27}Al MAS NMR observations (data not shown). All samples show the expected XRD features of HTs, including sharp and intense (00*l*) reflections at low 2θ values and less intense and asymmetric reflections at higher 2θ values. Indexing of the peaks is based on comparison to reported refined patterns of a 3R HT polytype.[34] The pronounced decrease in (00*l*) peak width and increased resolution for all peaks after hydrothermal treatment indicate increased structural order and parallels the increased particle size. The *d* spacing of the (003) reflection, which

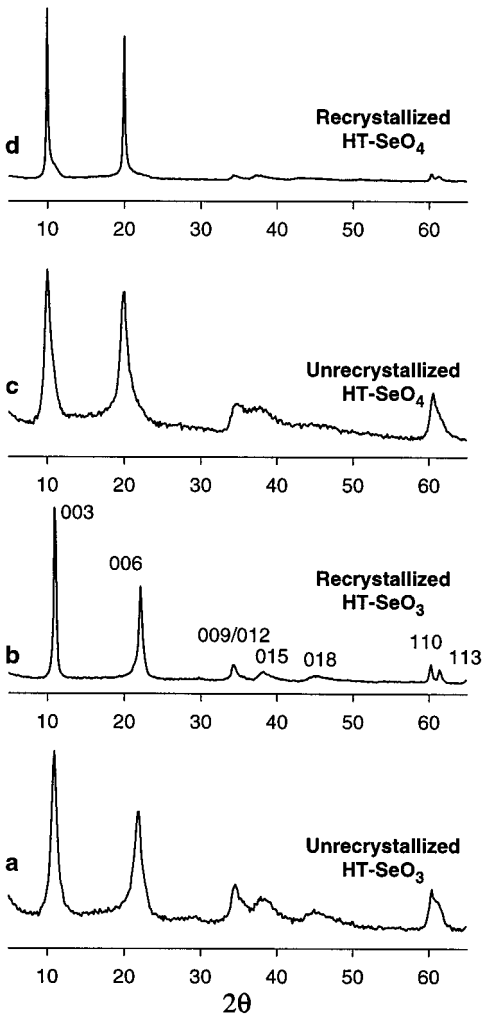

Figure 1. Powder XRD patterns for hydrotalcite-like compounds used in this study: (a) unrecrystallized HT-SeO_3, (b) recrystallized HT-SeO_3, (c) unrecrystallized HT-SeO_4, and (d) recrystallized HT-SeO_4.

corresponds to the thickness of a single unit structural layer, is 8.06 Å for HT-SeO_3 and 8.89 Å for HT-SeO_4. The (003) spacing for HT-SeO_4 is very similar to that of HT-SO_4 (8.9 Å).[35] In contrast to the observation for nitrate hydrotalcite,[10] recrystallization does not significantly change the *d* spacing of the selenate and selenite samples. The *a* cell parameter is 3.06 Å for all four samples based on the position of the (110) reflection ($a = 2d(110)$). This reflection is independent of layer stacking arrangement but does depend on the Mg/Al ratio.[1,34]

Paste and Dehydrated Hydrotalcites. To determine the effects of hydration/dehydration on interlayer *d* spacing, XRD patterns of the recrystallized HT-SeO_4 and HT-SeO_3 were recorded for their paste forms, at several times while the paste sample dried in air at room temperature, and after drying in air at 60 °C for 2 h (Figures 2 and 3). In a newly made paste, HT-SeO_4 is fully expanded to a $d = 11.16$ Å phase with an (003) peak as sharp as observed for the room humidity phase (Figure 2b). As water is lost, the 11.16 Å peak decreases in intensity and broadens (Figure 2b−e), an intermediate phase with $d = 10.06$ Å develops, and the original

(30) Louisnathan, S. J.; Gibbs, G. V. *Mater. Res. Bull.* **1972**, *7*, 1281.
(31) Louisnathan, S. J.; Hill, R. J.; Gibbs, G. V. *Phys. Chem. Miner.* **1977**, *1*, 53.
(32) Odom, J. D.; Dawson, W. H.; Ellis, P. D. *J. Am. Chem. Soc.* **1979**, *101*, 5815.
(33) Lide, D. R. *CRC Handbook of Chemistry and Physics*, 79th ed.; CRC Press: Boca Raton, FL, 1998.
(34) Bellotto, M.; Rebours, B.; Clause, O.; Lynch, J.; Bazin, D.; Elkaiem, E. *J. Phys. Chem.* **1996**, *100*, 8527.
(35) Bish, D. L. *Bull. Mineral.* **1980**, *103*, 170.

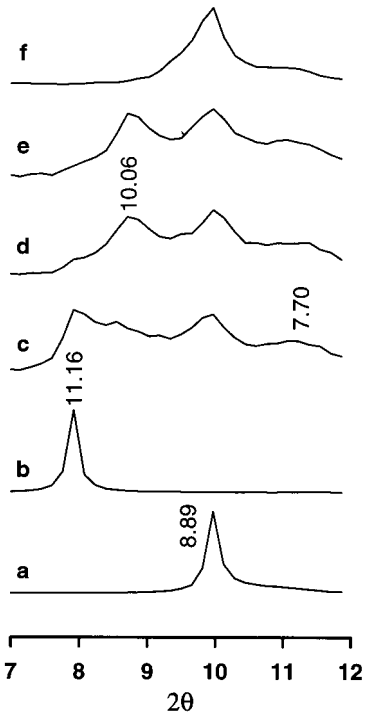

Figure 2. Time-resolved powder XRD patterns for recrystallized HT-SeO_4: (a) as made, room humidity; (b) fresh paste, room temperature; (c) 40 min drying at room temperature; (d) 76 min drying at room temperature; (e) 6 h drying at room temperature; and (f) 60 °C heated in air for 2 h. See text for description of experimental methods.

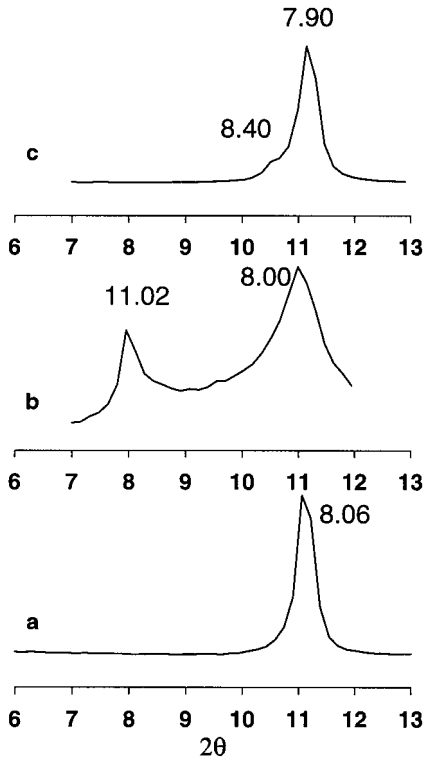

Figure 3. Time-resolved XRD pattern for recrystallized HT-SeO_3: (a) as made, room humidity; (b) fresh paste, room temperature; and (c) 3 h drying at room temperature. See text for description of experimental methods.

8.89 Å phase reappears and increases in abundance until the other two phases disappear (Figure 2f). The basal spacing expansion and contraction is reversible for repeated hydration/dehydration cycles. The basal spacing of the 11.16 Å phase indicates the presence of two water layers and the 8.89 Å spacing one. The basal spacing of 10.06 Å suggests that this phase is an ordered interstratification of the 11.16 and 8.89 Å phases. It could also be an intermediate phase in which the selenate anion has a different orientation than in the 8.89 Å phase, but orientation alone could make a difference of only 0.3 Å, as described in more detail below. The broadening of the reflections during drying is probably due dominantly to nonuniform dehydration. At RH = 0% (over P_2O_5), the basal spacing decreases to 8.53 Å, consistent with further loss of interlayer water. After exposure to ambient conditions (RH about 35%) for 24 h, it returns to 8.70 Å within 24 h.

Expansion and contraction of the basal spacings of HTs is rare, but is important for understanding the NMR results for HT-SeO_4. Bish[35] reported a Ni/Al sulfate HT phase having a *d* spacing of 8.9 Å at RH < 50% and 10.8 Å at RH > 50%, comparable to the spacings reported here. RH = 50% is also a key value for HT-SeO_4, as shown by the NMR data described below, and consistent with the similarity of SeO_4^{2-} and SO_4^{2-}. Bish[35] did not find a phase with an intermediate basal spacing, which may occur only in the transient conditions of our drying process.

For our samples, an invariant reflection at $2\theta = 11.3°$ occurs at all hydration/dehydration conditions used and is due to the HT-CO_3 contaminant. (The shoulders on the (003) and (006) reflections in Figure 1c and 1d also indicate the presence of this phase). The presence of two basal reflections indicates that the different anions tend to form distinct HT phases rather than a solid solution with both anions in all interlayers, although we cannot quantitatively determine the partitioning from the current data. This is a desirable result for studying selenate structure and dynamics in HTs using NMR, because the carbonate is less likely to affect the selenate. The observation also indicates that HT-CO_3 does not expand in response to increasing relative humidity, as previously shown by others.[1]

In contrast to HT-SeO_4, HT-SeO_3 does not expand at high RH or in a wet paste (Figure 3). This is the same behavior shown by HT-Cl and HT-NO_3 (our unpublished data). Segregation of SeO_4^{2-} and SeO_3^{2-} into separate phases is clearly shown for the recrystallized HT-SeO_3 sample in its paste form by the reflection at 11.02 Å (Figure 3b). This sample has significant SeO_4^{2-} due to oxidation, as discussed above. The 11.02 Å peak is at the position for expanded HT-SeO_4. It has much reduced intensity for the sample that was recrystallized prior to SeO_3^{2-} exchange and for the unrecrystallized sample, and thus clearly formed primarily by oxidation of SeO_3^{2-} during hydrothermal treatment.

TGA. TGA data (not shown) indicate that physically adsorbed and interlayer water are fully lost prior to 220 °C for HT-SeO_3 and 270 °C for HT-SeO_4. For the unrecrystallized samples, there is continuous water loss starting from room temperature. For the recrystallized samples, conspicuous weight-loss maxims occur at 110 °C for HT-SeO_3 and 195 °C for HT-SeO_4. The difference between the recrystallized and unrecrystallized samples is probably due to a greater range of water environments in the unrecrystallized samples due to their greater structural disorder and smaller particle sizes,

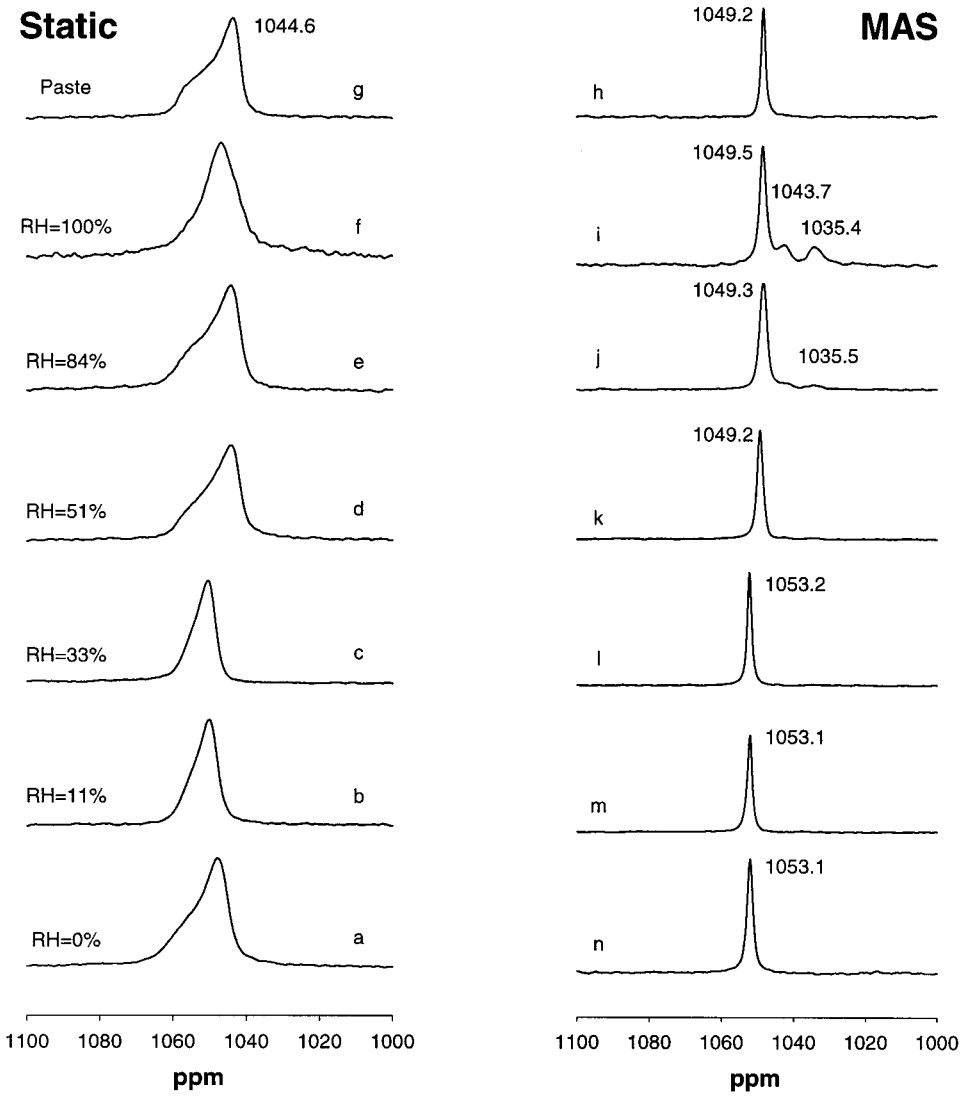

Figure 4. ^{77}Se NMR spectra of recrystallized HT-SeO_4 at room temperature and the indicated relative humidities (RH): left column, static spectra; right column, MAS spectra. See text for description of experimental methods.

consistent with the XRD and NMR data. Maximum dehydroxylation of the recrystallized samples occurs in two stages at 400 and 490 °C for both HT-SeO_4 and HT-SeO_3. These two events probably reflect loss of hydroxyls with different numbers of Al and Mg nearest neighbors. These are probably (1Al, 2Mg) at 400 °C and (3Mg) at 490 °C.[1,3] In contrast, the unrecrystallized samples yield only one dehydroxylation peak at ~480 °C, probably reflecting a less ordered Mg, Al distribution. Mass balance calculations suggest that Se is not lost below the maximum heating temperature of 650 °C used here. Our unpublished TGA data for HT-SO_4 up to 1100 °C show that sulfur is lost at 950 °C, and thus Se is expected to be lost in this temperature range or perhaps even higher.

^{77}Se NMR. *HT-SeO_4 at Variable Relative Humidity.* The room temperature (RT) static ^{77}Se NMR spectra of the recrystallized HT-SeO_4 sample show line shapes dominated by uniaxial chemical shift anisotropy (CSA) patterns at all relative humidities (Figure 4a−g), and the principal values of the CSA tensor change appreciably between RH = 33% and RH = 51%. Simulation of the spectra shows that at RH = 11% and 33% $\delta_{||}$ = 1057 ppm, $\delta_{\perp}$ = 1051 ppm, and δ_i = 1053 ppm. The 0% RH spectrum is broader but has the same isotropic chemical shift as at 11% and 33% RH. At RH = 51%, $\delta_{||}$ = 1057 ppm, $\delta_{\perp}$ = 1045 ppm, and δ_i = 1049 ppm. Importantly, the $\delta_{||}$ values, which represent the shielding along the unique axis of the uniaxial CSA tensors are independent of RH. The ^{77}Se MAS NMR data also show this transition. At the low RH, the peak maximum (= δ_i) is about 1053 ppm and at the higher RH = 1049 ppm, in agreement with the simulations of the static spectra. These δ_i values are very close to that of the 1 M Na_2SeO_4 solution (1051 ppm), clearly showing that there is no conversion of selenate to selenite. Because HT-SeO_4 is fully expanded into a two water layer structure in the wet paste (Figure 4 h), the 4 ppm change in δ_i from 1053.2 to 1049.2 ppm must be related to this expansion. The MAS spectra of the high RH samples also contain two small peaks at 1043.7 and 1035.4 ppm (Figure 4i, 4j, and 4k). These could correspond to surface species, to the 10.06 Å phase observed by XRD (Figure 2), or to $HSeO_4^-$ and/or $Se_2O_7^{2-}$ formed during long-term exposure to the RH buffer. The absence of adequate published data for the chemical shifts of Se-oxyanion species prevents us from fully interpreting these minor peaks.

The observed uniaxial CSA patterns for selenate indicate a distortion from the ideal tetrahedral symmetry due to external bonding effects. Isolated, ideal $^{77}SeO_4^{2-}$ tetrahedra would yield only a narrow, symmetric peak due to its T_d symmetry, as observed for aqueous solutions. Several studies of sulfate HT using FT-IR or Raman spectroscopy[5,36] have suggested that interlayer SO_4^{2-} is also distorted from tetrahedral symmetry. However, neither technique yields results as convincing and unambiguous as the NMR observations reported here. The distortion must be due to the combined effects of hydrogen bonding of the oxygens of the selenate to the OH of the octahedral layers and the H atoms of interlayer water molecules and to Coulombic interaction with the hydroxide layer. Resolving these contributions will require more comprehensive understanding of the ^{77}Se chemical shifts. The larger $|\delta_\perp - \delta_{||}|$ for the high RH samples implies a larger distortion. The unique symmetry axis of the SeO_4^{2-} ($\delta_{||}$) must be parallel to the *c* (perpendicular to the layer). Because $\delta_{||}$ does not change with changing RH, shielding in the direction perpendicular to octahedral sheet remains constant, whereas shielding parallel to the sheets (within the interlayer) varies. The observed change thus implies relatively large changes in H-bonding interaction with water molecules, but detailed interpretation will require better understanding of Se chemical shifts.

The observed ^{77}Se CSA patterns require preferred uniaxial orientation of the selenate. Such uniaxial symmetry could be obtained with either of two orientations, $C_2 \parallel c$ (two of the four oxygens up and two down) or $C_3 \parallel c$ (three oxygens up and one down, or the vice versa). A change in orientation from $C_2 \parallel c$ to $C_3 \parallel c$ would result in a calculated expansion of 0.30 Å along the *c* axis. On the basis of current data we cannot distinguish between the two possible orientations.

HT-SeO_4 at Variable Temperatures. Variable-temperature spectra for paste samples of the recrystallized HT-SeO_4 also show uniaxial CSA patterns (Figure 5a) except at −80 °C, where a triaxial CSA pattern is observed. For the uniaxial CSA patterns, the peak width ($|\delta_\perp - \delta_{||}| = \Delta\delta$) decreases progressively with increasing temperature from −60 to 98 °C. For example, at −40 °C the spectrum can be simulated with $\delta_\perp = 1038.2$ ppm, $\delta_{||} = 1061$ and 3.1 ppm line broadening, whereas that at 98 °C can be simulated with $\delta_\perp = 1055.5$ ppm, $\delta_{||} = 1047.7$ and 3.5 ppm line broadening. The uniaxial pattern is best defined (and thus simulated with the smallest line broadening) in the temperature range from −40 to 0 °C.

The decreasing $\Delta\delta$ with increasing temperature is best interpreted as being due to an increasing frequency of reorientational motion, as previously observed for surface and interlayer chloride in HT-Cl and hydrocalumite[9] and surface nitrate on HT-NO_3.[10] This motion must partially average the shielding anisotropy at Se, and must also involve relative motion of the SeO_4^{2-}, main layer OH groups and interlayer water molecules. The transition from triaxial Se symmetry at −80 °C to uniaxial symmetry at −60 °C is probably due to a dynamical order−disorder phase transition comparable to that we observed previously for HT-Cl and hydrocalumite.[9,37] We were unable, however, to obtain DSC data at this low temperature to demonstrate a thermodynamic effect. In this model the change from triaxial to uniaxial symmetry is due to a transition from a rigid interlayer structure to one in which the water molecules undergo dynamic, rotational (librational) disorder and make and break H-bonds with the interlayer anions.[9,37] In an ordered interlayer like hydrocalumite, each water molecule would have three nearest-neighbor anions but at any instant make only two H-bonds.[37] Librational motion of the water molecules on fixed structural sites allows for disorder over the three possible H-bonds. The decreasing uniaxial CSA, then, is due to diffusional hopping of anions and water molecules among interlayer sites, as we have proposed for the reduction in the ^{35}Cl

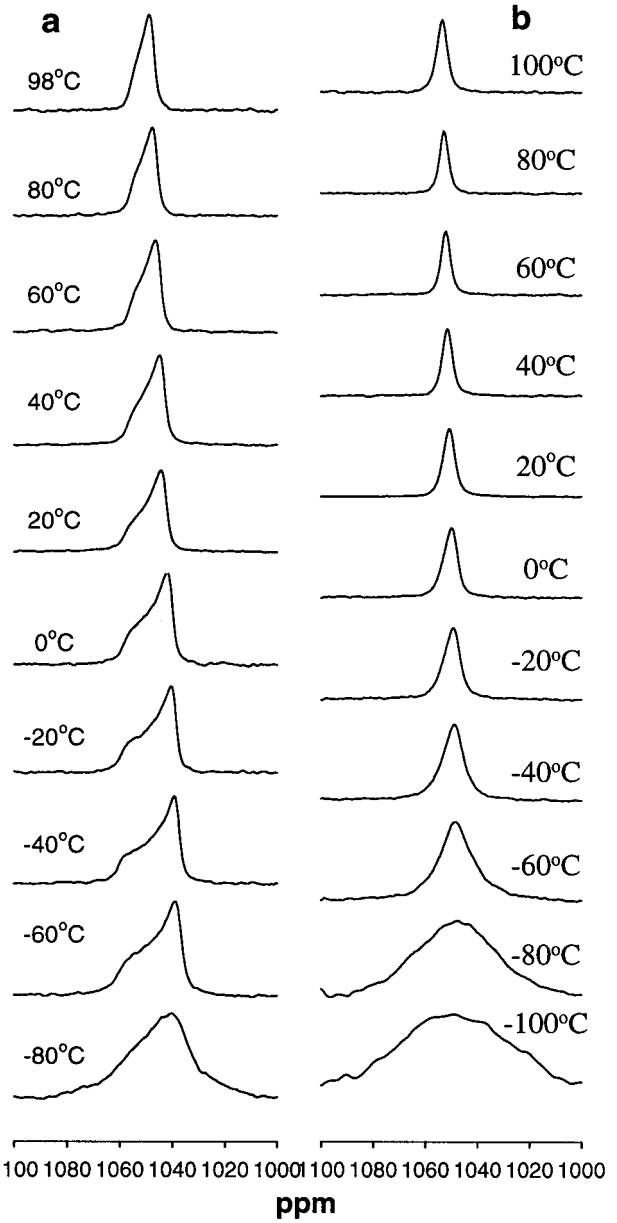

Figure 5. Static, in-situ variable-temperature ^{77}Se NMR spectra of (a) wet recrystallized HT-SeO_4 at the indicated temperatures and (b) room humidity unrecrystallized HT-SeO_4 at the indicated temperatures.

(36) Velu, S.; Ramkumar, V.; Narayanan, A.; Swamy, C. S. *J. Mater. Sci.* **1997**, *32* (4), 957.

(37) Kalinichev, A. G.; Kirkpatrick, R. J.; Cygan, R. T. *Am. Mineral.* **2000**, *85*, in press.

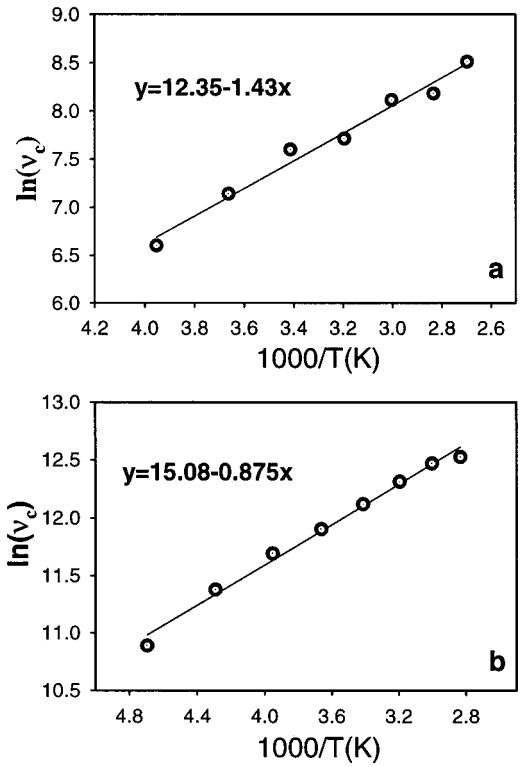

Figure 6. Temperature dependence of the selenate reorientational frequency for (a) recrystallized HT-SeO_4 and (b) unrecrystallized HT-SeO_4.

quadrupole coupling constant observed for hydrocalumite.[37] The frequency of the reorientation process that leads to the decreasing selenate CSA can be estimated from the temperature dependence of the NMR peak width[38,39] in the way we have previously used for surface nitrate on HT-NO_3.[10] The experimental line width, β, obeys the following equation:[38,39]

$$(\beta^2 - \beta_h^2)/(\beta_l^2 - \beta_h^2) = 2/\pi \arctan(\beta/\nu_c) \qquad (1)$$

where β_h and β_l are the smaller and larger limits for β, and ν_c is the reorientational frequency (1/correlation time), which varies with temperature as

$$\nu_c = \nu_0 \exp(-E_a/kT) \qquad (2)$$

We take β_h to be 147 Hz (fwhh of the MAS spectrum), and β_l to be the static peak width ($|\delta_\perp - \delta_{||}|$) at −60 °C (the lowest temperature at which the uniaxial CSA is observed), 1885 Hz. The reorientation frequency ν_c varies exponentially (Figure 6a), and at room temperature is ∼2000 Hz. The fit of ν_c to eq 2 yields an apparent activation energy E_a of 11.8 kJ/mol and a ν_0 of 2.3×10^5 Hz. This apparent activation energy is in the range expected for processes controlled by hydrogen bonding.[10,40−41] ν_0 is, however, 2 orders of magnitude smaller than that of surface nitrate at room humidity,[10] perhaps reflecting stronger Coulombic interaction due to the −2 charge of selenate and to a more confined interlayer environment.

The isotropic ^{77}Se chemical shifts move consistently to less shielded (more positive) values with increasing temperature, from 1044 ppm at −80 °C to 1046 ppm at −40 °C to 1050.3 ppm at 98 °C. This change is probably due to progressively decreasing hydrogen bonding to the selenate ion with increasing temperature. It is well-known that in aqueous solutions the instantaneous mean number of hydrogen bonds per water molecule decreases with increasing temperature,[41] and we expect similar changes in HT interlayers. Reduced hydrogen bonding would lead to stronger (more covalent) Se−O bonds within the ion, causing paramagnetic deshielding[42] at Se. In water, the reduction in the strength of the hydrogen bonding network results in decreasing viscosities. In HT interlayers, it leads to an increased rate of hopping of selenate and water molecules among sites. Similar hydrogen-bonding effects may also be responsible for the 4 ppm increase in isotropic chemical shift from high RH to low RH. On average, more hydrogen bonds are expected for the two water layer phase at high RH than for the one water layer phase at low RH.

In contrast to the results for the recrystallized sample, the variable-temperature ^{77}Se NMR spectra of the unrecrystallized HT-SeO_4 sample at room humidity (Figure 5b) contain a single symmetrical peak, with no indication of a CSA contribution of the peak shape. The peak width becomes progressively narrower with increasing temperature except at 100 °C, where it broadens slightly, probably due to lose of moisture. The lack of well-defined singularities is probably due to greater structural disorder (causing a wider range of interlayer environments) and a larger fraction of surface selenate. The peak width at −100 °C is much greater than for the recrystallized sample, consistent with this interpretation. The variation in peak width with temperature is much larger than for the recrystallized sample (Figure 5a), and we use upper and lower limits for eq 1 of 152 Hz (fwhh of the MAS spectrum) and 8755 Hz (fwhh of −100 °C spectrum). Thus, the reorientation frequencies obtained from eq 1 are 90−160 times larger than for the recrystallized sample at the same temperature (Figure 6), again consistent with a larger contribution of less tightly bound sites, many probably on the surface.[10] As expected, the apparent activation energy E_a = 7.2 kJ/mol (RH sample) is smaller than for the recrystallized sample (11.8 kJ/mol, paste sample), and $\nu_0 = 3.5 \times 10^6$ Hz, is larger. As for the recrystallized sample, the peak maximum for the unrecrystallized sample becomes progressively deshielded with increasing temperature.

HT-SeO_3 at Variable Relative Humidity. The ^{77}Se NMR spectra for HT-SeO_3 show peaks for selenite near 1200−1300 ppm and a smaller and variable amount of selenate near 1050 ppm (Figure 7). The water wetted (paste) sample (Figure 7, top) was prepared using a sample for which selenite was exchanged for chloride after hydrothermal treatment, and thus shows no selenate signal. The other spectra are for a sample that was selenate-exchanged and then recrystallized, and

(38) Gutowsky, H. S.; Pake, G. E. *J. Chem. Phys.* **1950**, *18*, 162−170.
(39) Moroz, N. K.; Afanassyev, I. S.; Fursenko, B. A.; Belitsky, I. A. *Phys. Chem. Miner.* **1988**, *25*, 282.
(40) Jonas, J.; Brown, D. *J. Colloid Interface Sci.* **1982**, *89*, 374.
(41) Kalinichev, A. G.; Bass, J. D. *J. Phys. Chem. A* **1997**, *101*, 9720.
(42) Mason, J. *Multinuclear NMR*; Plenum Press: New York, 1987.

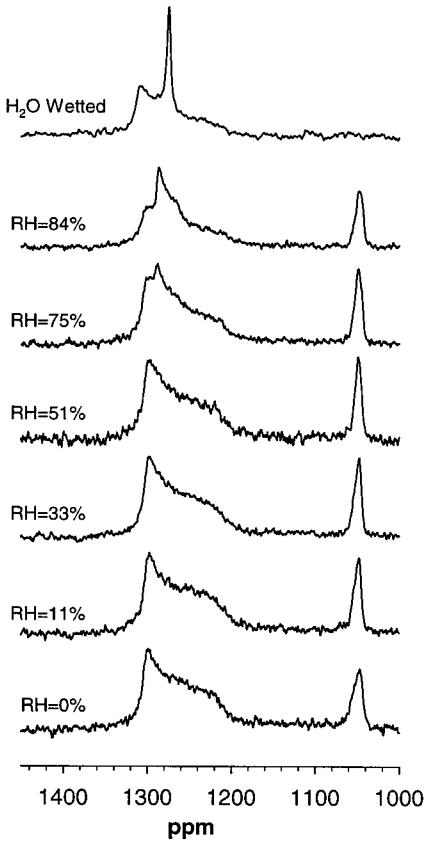

Figure 7. Static ^{77}Se NMR spectra of recrystallized HT-SeO_3 at room temperature and the indicated relative humidities (RH). See text for description of experimental methods.

thus contain signal for selenate formed during the hydrothermal treatment. As discussed above, the XRD data show the presence of separate selenite and selenate phases, and we now discuss only the selenite peaks. At low RH, the spectra show a broad uniaxial CSA pattern with $\delta_\perp = 1306$ ppm, $\delta_\parallel = 1215$ ppm, and $\delta_i = 1276$ ppm, consistent with the trigonal structure of selenite.[27] This CSA pattern remains unchanged up to RH = 75%, at which a narrow component appears near the center of the broad component. The intensity of this narrow component increases with increasing RH, and at RH = 84% it can be well-simulated with a uniaxial CSA pattern with $\delta_\perp = 1288$ ppm, $\delta_\parallel = 1261$ ppm, $\delta_i = 1279$ ppm, and a 7 ppm line broadening. The MAS spectrum of the RH = 84% sample shows these two peaks at chemical shifts identical to the simulated values (Figure 8). There is also a small component in the MAS spectra at 1302 ppm probably representing hydrated sodium selenite that precipitated from residual solution. For the fully hydrated paste sample, the broad component remains unchanged, whereas the narrow component is

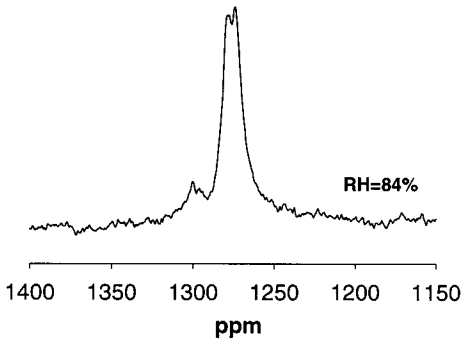

Figure 8. MAS ^{77}Se NMR spectrum of recrystallized HT-SeO_3 at room temperature and 84% RH.

an even narrower structureless symmetric peak at 1279 ppm (Figure 7, top).

These observations for HT-SeO_3 are very similar to those for nitrate hydrotalcite,[10] another nonexpanding HT compound. The broad, RH-independent component is assigned to interlayer selenite, and the narrow, RH-dependent component to selenite on exterior particle surfaces. At low RH, these components are unresolvable, consistent with both being rigidly held. Simulations of the spectra of the low RH samples require only one component to fully explain the spectra. As for HT-NO_3, the narrowing of the surface component at high RH is attributed to the averaging effects of dynamical reorientation as the amount of surface water increases. In contrast to nitrate, at 75% and 84% RH the selenite does not undergo rapid isotropic reorientation, but rather has a well-defined CSA pattern. Because the rigid selenite CSA is due primarily to its internal trigonal structure, this narrower CSA pattern must be due to a well-defined motion that partially averages the components of the CSA tensor. Full interpretation of this motion will require molecular modeling. Selenite undergoes isotropic averaging only for the paste sample, probably due to rapid exchange (exchange frequency $> 10^5$ Hz) between the surface and solution. The surface selenite also begins to undergo detectable dynamical averaging at much higher RH (75%) than nitrate (11%). We attribute this difference to the polarity and higher charge of selenite compared to nitrate. These two factors result in stronger interaction between the selenite and the hydroxide layer, and thus more surface water is required to activate fast reorientation.

Acknowledgment. This research is supported by the NSF grant EAR 95-26317, R.J.K. P.I. We thank Dr. Stephen Altaner for useful discussions. We also thank Dr. Duane Moore for help in collecting some of the XRD data.

CM990787W